



HAL
open science

Constructal design of thermochemical energy storage

Alexandre Malley-Ernewein, Sylvie Lorente

► **To cite this version:**

Alexandre Malley-Ernewein, Sylvie Lorente. Constructal design of thermochemical energy storage. International Journal of Heat and Mass Transfer, 2019, 130, pp.1299-1306. hal-02056376

HAL Id: hal-02056376

<https://hal.insa-toulouse.fr/hal-02056376>

Submitted on 26 Sep 2023

HAL is a multi-disciplinary open access archive for the deposit and dissemination of scientific research documents, whether they are published or not. The documents may come from teaching and research institutions in France or abroad, or from public or private research centers.

L'archive ouverte pluridisciplinaire **HAL**, est destinée au dépôt et à la diffusion de documents scientifiques de niveau recherche, publiés ou non, émanant des établissements d'enseignement et de recherche français ou étrangers, des laboratoires publics ou privés.

Constructal Design of Thermochemical Energy Storage

Alexandre Malley-Ernewein, Sylvie Lorente*

LMDC, Université de Toulouse, UPS, INSA, Toulouse, France

Abstract

This paper documents an analytical and numerical study of thermochemical energy storage in an open reactor. The analysis of the pressure losses and temperature distributions allows to predict what the geometrical features of the reactor should be. A numerical model simulating the thermochemical process is then presented and validated. In accord with the Constructal design methodology, the module configuration is morphed following the trends obtained in the analytical part, to head for better overall performances. The results show that the ratio between the heat produced by the chemical reaction within the entire module and the overall pumping power necessary to blow the fluid through the module increases as the imperfections reach equipartition. In terms of module configuration, this means (i) an increase in the number of salt layers and (ii) aspect ratios moving the module volume towards more compactness.

Keywords : Thermochemical energy storage, Constructal design, Compactness

* Corresponding author : lorente@insa-toulouse.fr

Nomenclature

Symbols

a	reaction advancement
A	surface, m ²
Be	Bejan number
c	concentration, mol/m ³
c_p	specific heat capacity, J/(kg K)
D	channel thickness, m
D_h	hydraulic diameter, m
D_v	diffusion coefficient of water vapor in air, m ² /s
f	friction factor
H	module height, m
H_{salt}	thickness of the salt bed, m
Δh	enthalpy of reaction, J/mol
K	salt permeability, m ²
k	thermal conductivity, W/(m K)
k_{cin}	kinetic reaction constant, 1/s
k_{st}	stoichiometric coefficient of the reaction

L	module length, m
\dot{m}	mass flow rate, kg/s
M_v	molar mass of vapor, kg/mol
n	number of salt layers and channels
n_s	bulk molar density, mol/m ³
p	pressure, Pa
p_v	partial water vapor pressure, Pa
p_{eq}	equilibrium pressure, Pa
\dot{q}	heat transfer rate, W
q'''	volumetric heat transfer rate, W/m ³
Re	Reynolds number
T	Temperature, K
t	Time, s
U	average fluid velocity, x axis, m/s
\mathbf{u}	velocity vector, m/s
V	average fluid velocity, y axis, m/s
\mathcal{V}	volume, m ³
x,y,z	coordinates, m

W module width, m

Greek symbols

α thermal diffusivity, m²/s

β ratio of heat released and pumping power

ε salt porosity

μ dynamic viscosity, Pa.s

ν kinematic viscosity, m²/s

ρ density, kg/m³

τ tortuosity

Φ module apparent porosity

Subscripts

eff effective

end end

in inlet

Max maximum

out outlet

salt salt

1. Introduction

Increasing the share of renewable energy in the energy mix is today an objective in most countries all over the globe. For example in Europe this share should represent 20% of the energy consumed by 2020 in order to cut the “dependence on imported fossil fuel and slash carbon emissions” [1]. Yet such target can only be reached if the issue of intermittency, and consequently energy storage, is overcome. Take the example of solar energy: the mismatch between energy production and energy consumption calls for thermal energy storage techniques in order to satisfy the consumer needs. This is true whatever the time scale considered. It can be short scale, a few hours for example, or it can be on a monthly scale [2], depending on the applications considered. The gap between production and consumption led to research in energy storage methods of several kinds: sensible, latent or thermochemical. The latter is typically summarized by: $Hydrate(s) + heat \leftrightarrow Deshydrate(s) + H_2O(vapor)$. The reaction involves a salt and its hydrate, and the energy released comes from the latent enthalpy and the bonds dissociation enthalpy during the hydration and dehydration processes. Such process presents the advantages of a high reaction heat compared to latent or sensible storage. Thermochemical energy storage is not concerned by the issue of heat leakage which represents an additional advantage, and explains the strong research interest received [3–9].

The Constructal law was stated for the first time in 1996 [10], and explored in many domains since [11–22]. From the design of efficient cooling systems [11–13] or boilers [14] to underground heat exchangers [15–17], the approach provided by the Constructal law is an opportunity to discover efficient configurations. The universality of Constructal design was addressed in [18,19] with applications in mass transfer: natural diffusion, or ionic transport driven by electrical driving forces. An overview of the Constructal law can be found in [20–22]. In the field of thermal energy storage, latent and sensible storage were covered in [23–25] for large scale systems showing the impact of tree-shaped structures on the results. Special

attention was given to Constructal design with fins in [26–28]. Constructal latent energy storage for building applications can be found in [29–31]. The design methodology was applied to one single salt-gradient solar pond (SGSP) then extended to an entire SGSP field in [32]. Finally, an exergy approach to the problem is given in [33].

Here, we are interested in thermochemical energy storage modules, envisaged as flow systems which architecture can evolve in time towards better designs. We document the design of a compact thermochemical energy storage system. In this work, fixing the total volume of the reactor, the shape evolves in such a way that the entire system performs at best with maximum heat transfer and minimum pumping power. The search is not random. In Constructal design we start by identifying the dominant mechanisms and trends. This is why the first part of this article is about the theoretical analysis of the configuration.

2. Analysis

2.1. Pressure losses

The chemical energy storage unit is a parallelepiped with fixed volume $\mathcal{V} = WLH$. The volume of salt is also fixed, and given by $\mathcal{V}_{salt} = nH_{salt}WL$, where n is the number of salt elements (n is an even number). Fluid channels of thickness D are inserted between each salt bed. We have $H = n(H_{salt} + D)$ as the channels at the two ends of the WLH volume have a thickness $D/2$, see Fig. 1. In sum, the volume WLH is a designed porous system made of reactive salt elements sandwiched between fluid channels. In this open process, the heat transfer fluid (humid air) enters from the left and follows the channels which ends are obstructed, forcing the fluid to pass through the 2 adjacent salt beds. The heat transfer fluid sweeps the salt, allowing the chemical reaction to happen, and heat to be stored or released. At the exit of the salt bed, the fluid is again

channeled to reach a new slot which one end is closed, and the flow exits on the other side of the module. The total mass flow rate is fixed, it is given by $\dot{m}_{total} = n \times \dot{m}$.

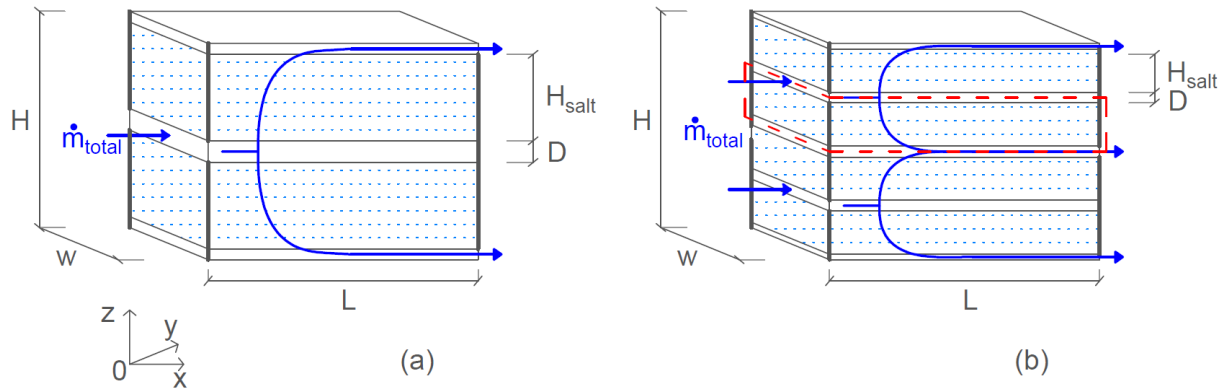


Figure 1 Sketch of the thermochemical energy storage module, with 2 salt beds (left), and 4 salt beds (right).

The design of the reactor must meet several requirements: the entire volume of salt must react within a prescribed time frame, provide the requested heat (if we consider winter conditions), and allow the fluid temperature in the exit channel to be at a specified value. The preheated fluid can then be blown into the building air conditioning system. The key question is how to allocate the salt volume within the chemical energy storage unit: How many fluid channels should be present? How should H_{salt} be chosen so that the overall heat released/stored during hydration corresponds to the objective within the given time frame? We look here for maximum heat, minimum pressure losses, while the losses due to the kinetic of the chemical reaction should be minimum.

We start analyzing the main features of the designed thermochemical storage system by considering first that W is fixed. The thermochemical energy storage system is described in Fig. 1. The domain delimited by the dashed line represents an elemental module made of one slab of salt sandwiched between one entrance channel and one exit channel, the thickness of which is $D/2$ due to symmetry. We consider that, if the mass flow rate entering the channel is \dot{m} , then $\dot{m}/2$ is the mass flow rate through one salt bed. The fluid enters the channel at a temperature T_{in} . Remember that the reactive salt total volume is fixed because a specific power is expected. The thickness H_{salt} is unknown. Consequently the surface of exchange $A_s = L \times W$ will depend on the value of H_{salt} . The design parameters are the geometrical characteristics of the fluid slots, the salt element geometry, while the module and salt volumes are fixed. Assume that the mass flow rate available for one single salt bed ($\dot{m}/2$) decreases linearly to $\dot{m}(L) = 0$. We assume that the variation of the mass flow rate can be treated as continuous.

Therefore

$$\dot{m}(x) = \dot{m} \left(1 - \frac{x}{L}\right) \quad (1)$$

At the abscissa x the pressure loss is:

$$dp(x) = f \frac{1}{2} \rho U^2 \frac{4dx}{D_h} \quad (2)$$

where f is the friction factor $f = 24(D^2 + W^2)/[Re_{D_h}(D + W)^2]$, Re_{D_h} is the Reynolds number based on the hydraulic diameter D_h , ρ is the fluid density and U is the average velocity of the fluid. The hydraulic diameter is $D_h = 2DW/(D + W)$ in the case of a rectangular cross section [34].

Combining Eqs. 1 and 2 together, we write:

$$\Delta p = \int_0^x \frac{12\nu(D^2 + W^2)}{A^3} \dot{m} \left(1 - \frac{x}{L}\right) dx \quad (3)$$

where ν is the kinematic viscosity, $A = DW$ is the channel cross section. As a result,

$$\Delta p(x) = \frac{12\nu(D^2 + W^2)}{A^3} \dot{m} \left(1 - \frac{x}{2L}\right) x \quad (4)$$

Here Δp is the overall pressure loss between the entrance and the end of the same channel.

2.2. Temperature along an entrance channel

The analysis continues by considering the fluid temperature change along the inlet channel. While the gas flows along the channel, it also feeds the porous material and the chemical reaction takes place within the salt. The heat released by the hydration warms also the gas in the channel. For the reaction to happen, the temperature (and pressure) must remain below a threshold which corresponds to the equilibrium conditions given by Clausius-Clapeyron equation [35]. This limitation decides the channel length, together with the criterion on minimum pressure losses. The fluid enters the channel at T_{in} and while flowing along the channel of length L , its temperature increases due to the chemical reaction in the salt. Consider a channel element of thickness dx with dx infinitely small. The gas flows through the elemental volume of cross section $D \times W$ and thickness dx . At the 2 interfaces Wdx of the elemental volume, the salt hydration generates heat. Energy conservation requires

$$\dot{m}(x)c_p dT = q''' W z dx \quad (5)$$

where z is the thickness of hydrated salt.

The increase of energy due to the chemical reaction is $\frac{dc}{dt} \Delta h$, where c is the concentration of the reactive species, and Δh is the enthalpy of reaction. $\frac{dc}{dt}$ can be replaced by $n_s \frac{da}{dt}$ where n_s represents the molar density of the reactive salt and a is the advancement of the chemical reaction. As an example we use the expression provided in [36] where the advancement a represents the ratio of species reacting with the salt at time t , and the total amount of species reacting at complete hydration of the salt we write:

$$\frac{da}{dt} = k_{cin} \left(1 - \frac{p_{eq}}{p_v}\right) (1 - a) \quad (6)$$

where k_{cin} is the kinetic constant, p_v is the vapor pressure, and p_{eq} is the equilibrium gas pressure. The latter is a function of the temperature through the Clausius-Clapeyron equation [35].

Equation 6 is the advancement rate equation for a salt hydrated by the vapor contained in a flow of humid air. Considering that vapor is a perfect gas, the vapor pressure can be expressed as a function of the reaction advancement and the temperature, $p_v = c_{Tot} R_v T a$, where c_{Tot} is the total number of mole of vapor reacting with the salt per volume of salt, when $a = 1$, and R_v the vapor constant. For a given value of the advancement,

$$\dot{m} \left(1 - \frac{x}{L}\right) c_p dT = n_s \Delta h z W k_{cin} (1 - a) \left(1 - \frac{p_{eq}(T)}{c_{Tot} R_v T a}\right) dx \quad (7)$$

We consider as a first approximation, that the thickness of hydrated salt varies linearly with the channel length, $z = H_{salt} (1 - x/L)$. Writing that $A_1 = c_{Tot} R_v a$, and $A_2 = (n_s \Delta h H_{salt} W k_{cin}) (1 - a) / \dot{m} c_p$, we have:

$$\int_{T_{in}}^T \frac{1}{1 - A_1 \frac{p_{eq}(T)}{T}} dT = A_2 \int_0^x dx \quad (8)$$

The solution of Eq. 8, obtained numerically, shows that the temperature increases with the channel length. It is discussed later in the paper.

2.3. Temperature at the exit of the module

Next, we move to the salt bed and write that the total heat transfer rate through the salt slab of thickness H_{salt} is $\dot{q} = \frac{\dot{m}}{2} c_p (T_{out} - T_{in})$, considering that the order of magnitude of the fluid temperature at the slab entrance is T_{in} , and T_{out} is the fluid temperature at the exit of the salt bed. Assuming Darcy flow through the reactive porous medium, the average velocity is $V = \frac{K}{\mu} \frac{\Delta p}{H_{salt}}$, where K is the salt permeability, Δp is the pressure difference through the salt.

The mass flow rate is given by $\frac{\dot{m}}{2} = \rho V W L$. Finally, the total heat transfer rate is

$$\dot{q} = \rho \frac{K \Delta p W L}{\mu H_{salt}} c_p (T_{out} - T_{in}) \quad (9)$$

Equation 9 can also be written as

$$\dot{q} = k_{eff} Be \frac{W L}{H_{salt}} (T_{out} - T_{in}) \quad (10)$$

where $Be = K \Delta p / \alpha \mu$ is the Be number for porous media [37], where α is thermal diffusivity and k_{eff} is the porous material thermal conductivity obtained from the salt porosity ε , the salt

and fluid thermal conductivities, respectively k_{salt} and k : $k_{eff} = (1 - \varepsilon)k_{salt} + \varepsilon k$. Finally,

from $\dot{q} = \frac{dc}{dt} \Delta h WLH_{salt}$ we obtain:

$$T_{out} - T_{in} = \frac{n_s \Delta h H_{salt}^2}{k_{eff} Be} k_{cin} \left(1 - \frac{p_{eq}}{p_v}\right) (1 - a) \quad (11)$$

Or, in a non-dimensional form

$$\tilde{T}_{out} = \frac{1}{Be} \left(1 - \frac{p_{eq}}{p_v}\right) (1 - a) \quad (12)$$

where $\tilde{T}_{out} = [(T_{out} - T_{in})k_{eff}] / (n_s \Delta h H_{salt}^2 k_{cin})$.

The evolution of the temperature at the exit of the salt bed as a function of the reaction advancement is plotted in Fig. 2. Here we accounted again for the equilibrium pressure variation with the temperature through the Clausius-Clapeyron equation [35]. Figure 2 highlights the impact of the Be number on the exit temperature from the start of the salt hydration process ($a = 0$) to its end ($a = 1$). The lower the Be number, the higher the fluid temperature obtained at the exit of the salt layer and therefore at the exit of the module.

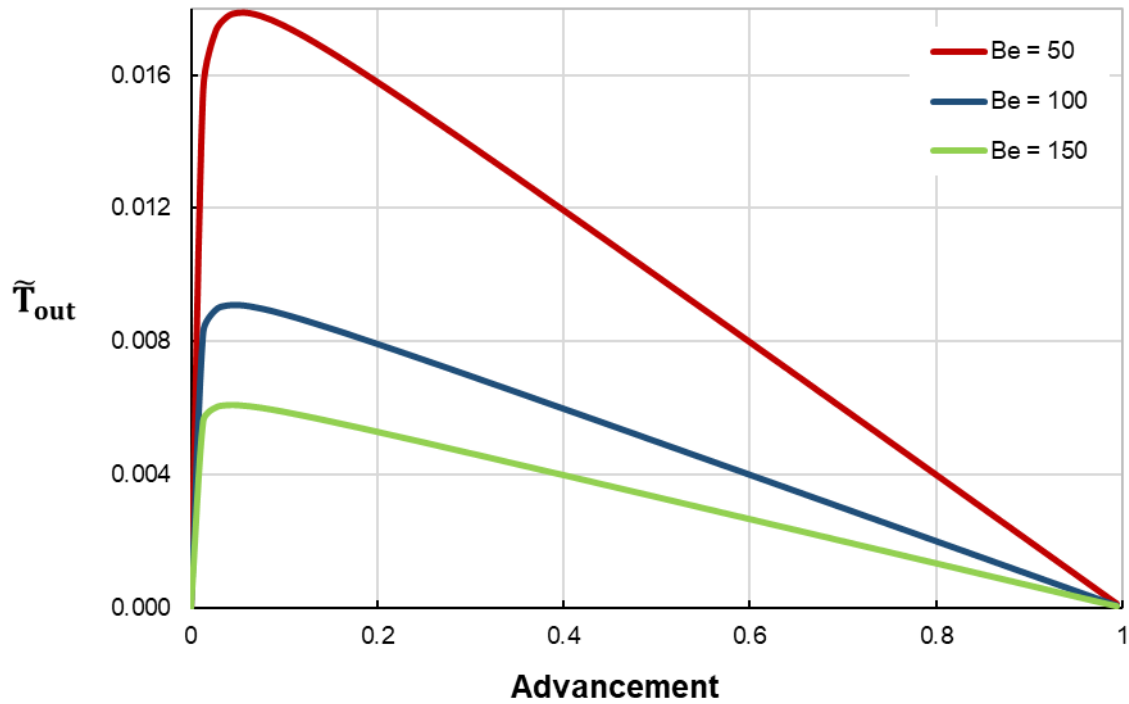


Figure 2 Non dimensional temperature \tilde{T}_{out} at the exit of a salt bed for various values of the Be number.

3. Model

From the trends obtained in the previous section, a numerical model was developed in order to describe the heat and mass transfers through the entire elemental system, namely: entrance channel, reactive porous material, exit channel. We model an open system made of a salt reacting with the water vapor contained in air. Mass conservation for the humid air (Eq. 13) and for vapor (Eq. 14) were solved in the entrance and exit channels. In the salt, mass conservation for humid air and vapor accounts for the mass source/sink due to the salt dehydration/hydration (Eqs. 15 and 16). Note that Eq. 14 is necessary because vapor transport must be expressed in the salt to determine the mass source/sink for the chemical reaction. Therefore vapor transport

is written within the entire domain (salt and channels). Momentum conservation is described by the Navier-Stokes equations for laminar flow in the channels (Eq. 17). We solve the Brinkman equation (Eq. 18) as we need to couple the flow in the channels described by the Navier-Stokes equations, and the flow through the salt which porosity ε is high enough to justify the use of the Brinkman equation. Finally, energy conservation is written within the channels (Eq. 19) and in the salt (Eq. 20). Equation 20 accounts for the heat source/sink created by the chemical reaction.

$$\frac{D\rho}{Dt} = 0 \quad (13)$$

where ρ is the humid air density.

$$\frac{Dc}{Dt} + \nabla(-D_v \nabla c) = 0 \quad (14)$$

where c is the water vapor concentration, and D_v is the vapor diffusion coefficient.

$$\varepsilon \frac{\partial \rho}{\partial t} + \nabla(\rho \mathbf{u}) = -k_{st} n_s \frac{da}{dt} M_v \quad (15)$$

where \mathbf{u} is the velocity vector, M_v is the molar mass of vapor, and k_{st} is the stoichiometric reaction coefficient.

$$\varepsilon \frac{\partial c}{\partial t} + \nabla(-D_{eff} \nabla c) + \mathbf{u} \nabla c = -k_{st} n_s \frac{da}{dt} \quad (16)$$

where D_{eff} is the effective diffusion coefficient of the water vapor in the air inside the porous medium, $D_{eff} = \varepsilon^{4/3} D_v$, according to the Millington and Quirk model [38].

$$\rho \frac{D\mathbf{u}}{Dt} = -\nabla p + \mu \nabla^2 \mathbf{u} \quad (17)$$

$$\rho \frac{D\mathbf{u}}{Dt} = \varepsilon \left[-\nabla p + \mu \nabla^2 \mathbf{u} + \frac{\mu}{K} \mathbf{u} \right] \quad (18)$$

$$\rho c_p \frac{DT}{Dt} + \nabla \cdot (k \nabla T) = 0 \quad (19)$$

$$(\rho c_p)_{eff} \frac{\partial T}{\partial t} + \rho c_p \mathbf{u} \cdot \nabla T + \nabla \cdot (k_{eff} \nabla T) = n_s \frac{da}{dt} \Delta h \quad (20)$$

where $(\rho c_p)_{eff}$ and k_{eff} are given by

$$(\rho c_p)_{eff} = (1 - \varepsilon) \rho_{salt} c_s + \varepsilon \rho c_p \quad (21)$$

where c_s is the heat capacity of the salt. da/dt is given by Eq. 6.

The imposed boundary conditions are constant in time. The fluid enters at a fixed temperature T_{in} and vapor concentration c_{in} . The inlet mass flow rate is \dot{m} , assuming an entrance length greater than $0.05 Re_{D_h}$ for fully developed flow [39]. At the outlet, the fluid is at atmospheric pressure. It exists at temperature and vapor pressure resulting from the heat and mass exchanges within the module. All the other external boundary conditions are of thermal insulation, no-slip for the fluid mechanics aspect, and zero vapor flux.

Initially, the fluid is static at atmospheric pressure, the temperature of the entire system is T_0 , and the vapor concentration is c_0 . c_0 is the concentration of vapor corresponding to the equilibrium vapor pressure at temperature T_0 .

The entire system of equations was solved thanks to a FEM software [40]. A specific study on the mesh accuracy was implemented with mesh refinement until energy and mass conservation were obtained.

4. Validation

The results for the salt bed were compared to the experimental data obtained by Ref. [41]. The salt bed made of SrBr_2 was submitted to 7 cycles (hydration and dehydration). We used the data from the 3 first hydrations and dehydrations for validation. The salt bed was a parallelepiped, where $H_{\text{salt}} = 7.5$ cm, $L = 65.1$ cm, $W = 69.4$ cm. Table 1 provides the initial conditions used during the different simulations [41]. The model input are the moist air temperature, the vapor pressure and the volumetric air flow, the experimental kinetic reaction constant, together with the material properties. Table 2 gives the salt characteristics.

We considered that the porous medium characteristics evolve with the hydration state, following the experimental data in [41]. The porosity, density, thermal capacity vary linearly with the reaction advancement. The thermal conductivity was kept constant. The porous media permeability K changes linearly with the advancement, during dehydration, while during hydration it is calculated using [35]:

$$K = \left[\frac{1-a}{K_{a=0}} - \frac{a}{K_{a=1}} \right]^{-1} \quad (22)$$

where $K_{a=1}$ is the salt bed permeability at full hydration ($a = 1$), and $K_{a=0}$ is the salt bed permeability at full dehydration ($a = 0$).

Table 1 : Experimental input data (adapted from [41])

	Inlet temperature T_{in} (°C)	Inlet vapor pressure $p_{v, \text{in}}$ (Pa)	Inlet volumetric flow rate (m ³ /h)	Kinetic constant k_{cin} (s ⁻¹)
1 st dehydration	80.0	2557.0	312.6	$8 \cdot 10^{-6}$
1 st hydration	25.0	997.5	289.6	$8 \cdot 10^{-6}$
2 nd dehydration	77.9	2570.0	311.2	$3.5 \cdot 10^{-6}$
2 nd hydration	25.0	981.0	290.0	$5.5 \cdot 10^{-6}$
3 rd dehydration	79.8	2459.0	313.0	$1.4 \cdot 10^{-6}$
3 rd hydration	25.0	944.7	290.0	$3 \cdot 10^{-6}$

Table 2 : Salt characteristics (adapted from [36, 41])

heat capacity	$c_{salt,a=0}$, J/(kg K)	456
	$c_{salt,a=1}$, J/(kg K)	968
permeability	$K_{a=0}$, m ²	$5.7 \cdot 10^{-10}$
	$K_{a=1}$, m ²	$5.9 \cdot 10^{-11}$
enthalpy of reaction	Δh , J/mol	$3.37 \cdot 10^5$
entropy of reaction (necessary in the Clausius-Clapeyron equation)	Δs , J/(mol K)	875
porosity	$\epsilon_{a=0}$	0.684
	$\epsilon_{a=1}$	0.383
thermal conductivity	k_s , W/(m K)	1
density	$\rho_{salt,a=0}$, kg/m ³	3481
	$\rho_{salt,a=1}$, kg/m ³	2390

We present in Fig. 3 the advancement history during 3 sequences of salt hydration/dehydration.

The numerical results match very well the experimental ones, validating the model.

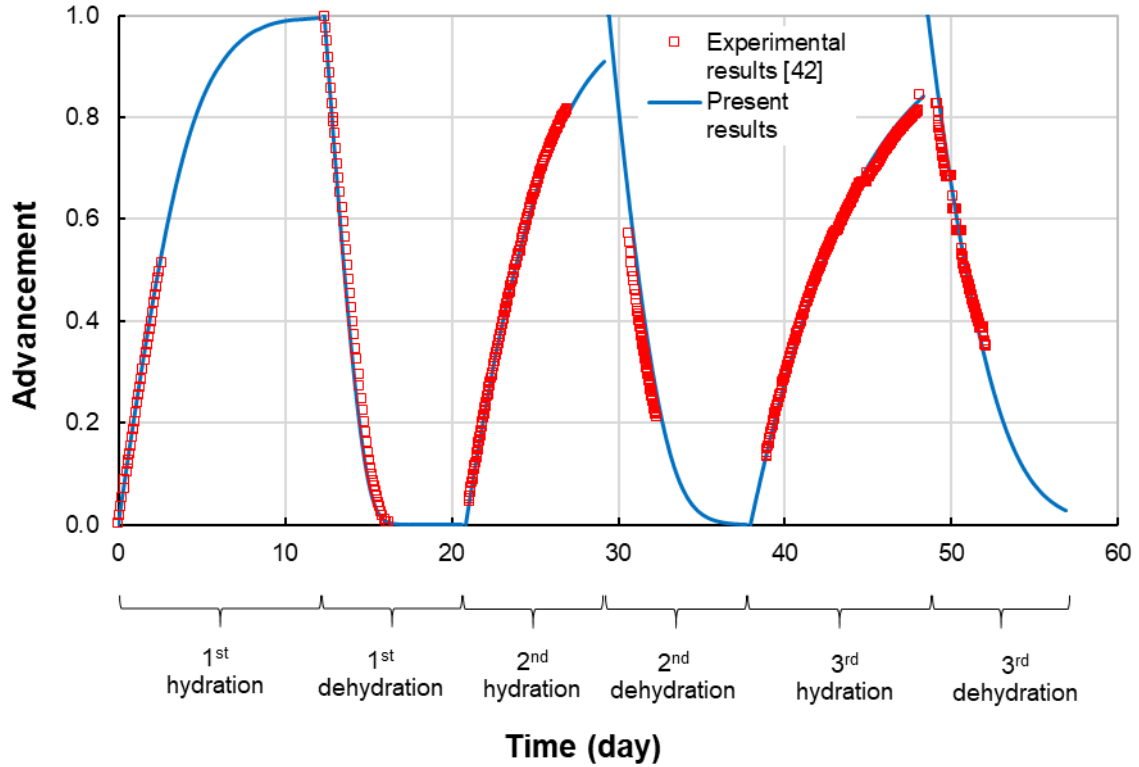


Figure 3 Reaction advancement as a function of time, for 3 cycles of hydration-dehydration, comparison with experimental results.

5. Constructal design

5.1 Salt layers

We consider the fixed volume WLH containing a fixed volume of salt. As the volume of salt is given by $\mathcal{V}_{salt} = nWLH_{salt}$, the designed porous system has an apparent porosity $\Phi = 1 - nH_{salt}/H$. In this work, the apparent porosity is 20%. First we fix H , W and L ($H = 12.5$ cm, $W = 10$ cm and $L = 8$ cm) and vary the number of salt layer. Accordingly the number of air channels also varies together with their thickness. The total mass flow rate, the inlet temperature and the inlet relative vapor pressure of the humid air are fixed ($\dot{m}_{total} = 0.89$ m³/h, $T_{in} = 25^\circ\text{C}$, $p_{v,in} = 997.5$ Pa). We show here a hydration case. The number of salt layers varies evenly from 2 to 12. The material characteristics are the ones given in Table 2.

In order to compare the numerical results with the theoretical ones proposed in Section 2, we extracted the pressure values along the entrance channel when x varies between 0 and L . The results are plotted in a non-dimensional way in Fig. 4: $\Delta\tilde{p} = \Delta p / \Delta p_{max}$, where Δp_{max} is the maximum value of pressure obtained for $n = 12$ salt beds at $x/L = 1$. The shape of the pressure loss corresponds to the analytical result; the discrepancy between the predictions provided by Eq. 4 and the numerical results tends to decrease when the number of salt layers increases. Indeed, when n increases, $D/L \ll 1$ which makes the air channel slender and closer to the assumption of a 1D pressure losses taken in the theoretical approach of Section 2.

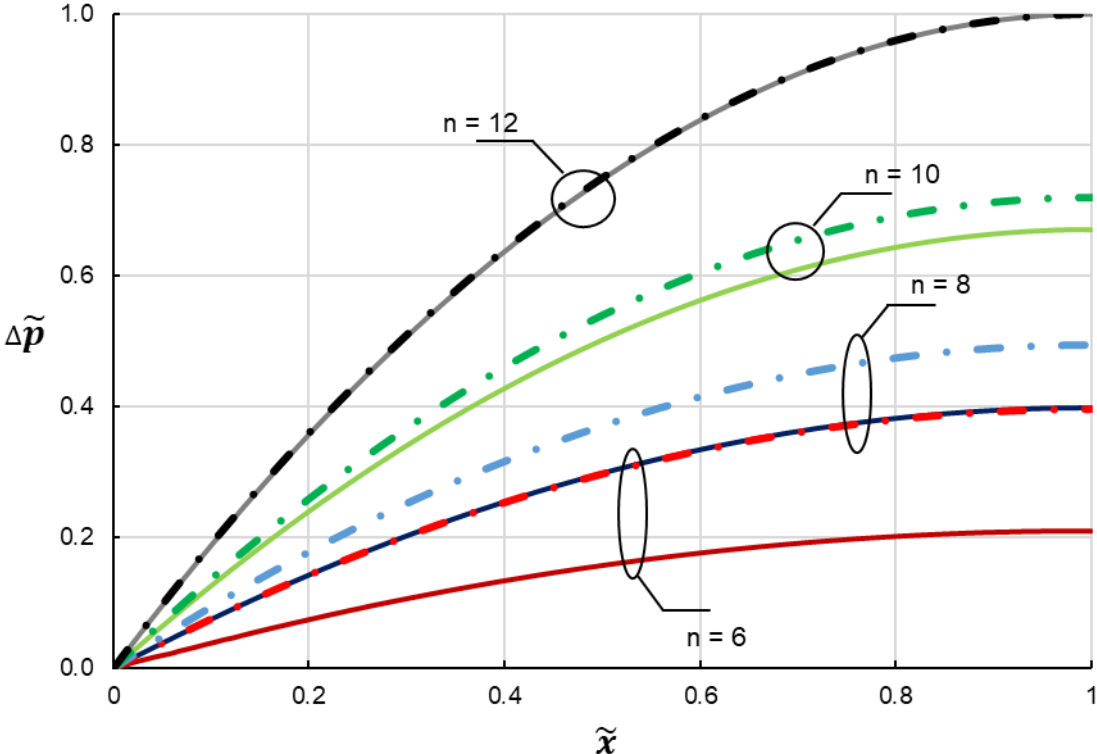


Figure 4 Non-dimensional pressure losses $\Delta\tilde{p}$ along an entrance channel, numerical (—) and theoretical results (- · -).

We show in Fig. 5 the ratio of pressure losses through one salt bed and the total pressure losses (from the channels inlet to the outlet cross section). The results come from the numerical model which simulated the entire 2D problem. The non-dimensional time is $\tilde{t} = t/t_{max}$, where t_{max} is the time for an advancement $a = 1$. Most of the pressure losses are located in the salt. Yet the ratio decreases when the number of salt layer increases (smaller values of H_{salt}). Note that the ratio is not a constant. As time increases the salt properties change with its hydration leading to smaller values of the permeability and porosity.

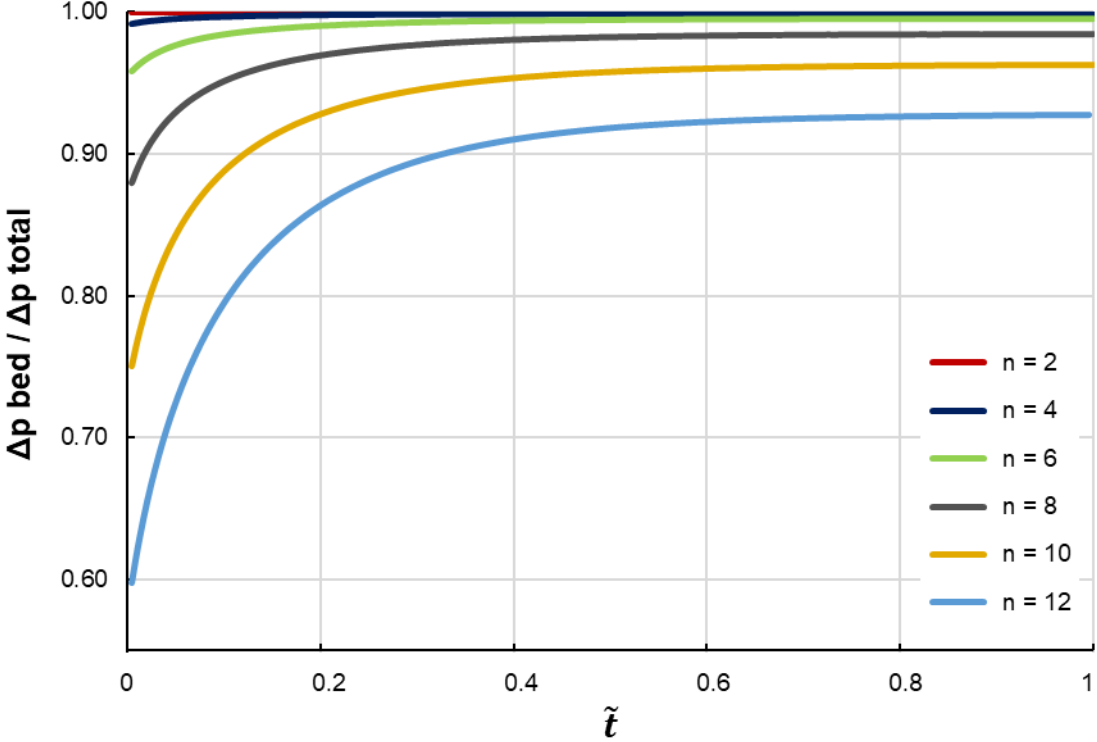


Figure 5 Pressure losses ratio as a function of time, numerical results. W, L and H are constant, $n = 2, 4, 6, 8, 10$ and 12 bed layers.

Figure 6 exhibits the air temperature plotted in a non-dimensional way, $\tilde{T} = (T - T_{in}) / (T_{max} - T_{in})$, along the entrance channel. T_{max} is calculated from the Clausius – Clapeyron equation assuming that the equilibrium pressure is the one corresponding to the inlet pressure at T_{in} at the channel entrance. In both cases T is the channel bulk temperature. The theoretical results were obtained from the integration of Eq. 8, while the numerical results correspond to the temperature extracted at mid thickness ($D/2$) and along the channel. The numerical profile corresponds to the case $n = 12$ as it is closer to the one-dimension flow assumption in the channel. In this example, $a = 0.5$. Similar agreement was found between the analytical results and the numerical ones for the other advancement values. The fluid temperature increases due to the chemical reaction that surrounds the air duct. Nevertheless in this particular case, the maximum temperature that would prevent the reaction to happen is never reached, which means that increasing the channels length is a degree of freedom in the design.

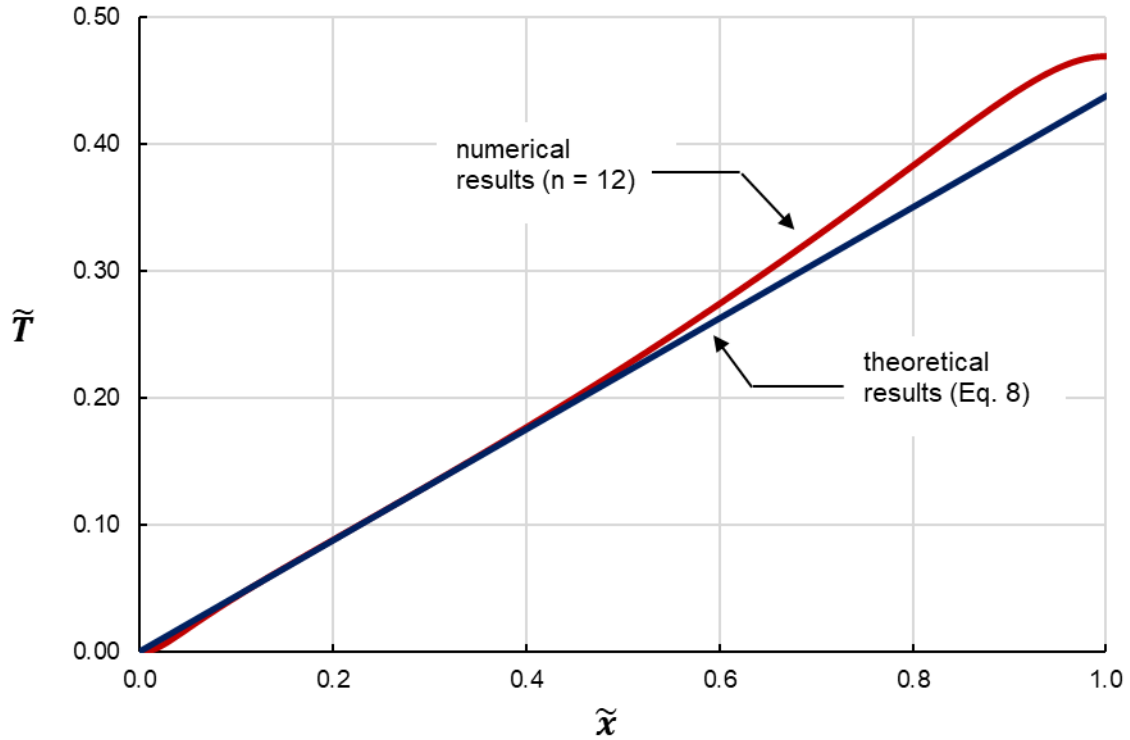


Figure 6 Non-dimensional temperature \tilde{T} along an entrance channel. Comparison between theoretical results and numerical ones ($n = 12$ salt beds), $a = 0.5$.

Next, we show in Fig. 7 the ratio between the heat produced by the chemical reaction within the entire module ($n_s \frac{da}{dt} \Delta h$ over the salt volume) and the overall pumping power necessary to blow the fluid through the module, β . β was calculated from the numerical results. The β ratio decreases in time whatever the number of salt layers. Yet, the effect of the configuration is clearly highlighted in Fig. 7: splitting the salt volume into an increasing number of salt beds in parallel allows to obtain a much higher ratio. The impact is not through the heat released by the salt hydration, which is basically not dependent on n , but on the pumping power which decreases with the pressure losses. This result is an illustration of the Constructal law: the best design corresponds to the equipartition of imperfections. Here the best design emerges when

the pressure losses through the salt are of the same order of magnitude as the pressure losses along the channels for fixed H , L and W , and a number of salt layers free to vary.

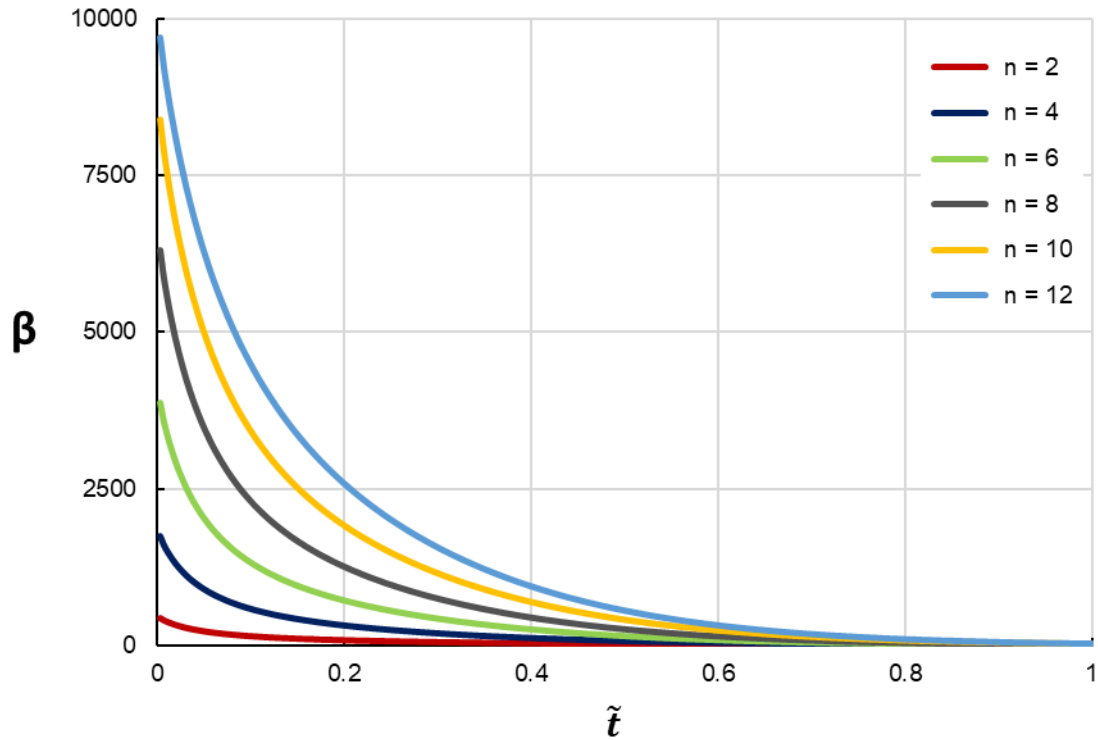


Figure 7 Ratio of heat released and pumping power, β , as a function of time.

5.2 Shape of the module

We add more degree of freedom in the design of the module by allowing H , L and n to vary while the total volume remains fixed and the module designed porosity is kept at a value $\phi = 20\%$.

Looking for equipartition in the distribution of imperfections, we write:

$$\Delta P_L \sim \Delta P_{Hsalt} \quad (23)$$

From Eq. 4, we calculate ΔP_L :

$$\Delta P_L = \Delta P(L) = \frac{12\nu(D^2 + W^2)}{A^3} \dot{m} \frac{L}{2} \quad (24)$$

while ΔP_{Hsalt} can be estimated from Eq. 9. As $\dot{q} = \frac{\dot{m}}{2}(T_{out} - T_{in})$, Eq. 23 becomes

$$12K \sim \frac{\phi^3(1 - \phi)H^4\mathcal{V}^2}{n^2L^2[(\phi LH^2)^2 + (n\mathcal{V})^2]} \quad (25)$$

Using the geometrical parameters corresponding to Section 5.1, we plotted Eq. 25 in Fig. 8 as a function of the number of salt beds. When $n \geq 10$ the difference between the two terms starts vanishing: the configuration allows an equipartition of the imperfection (here, the pressure losses).

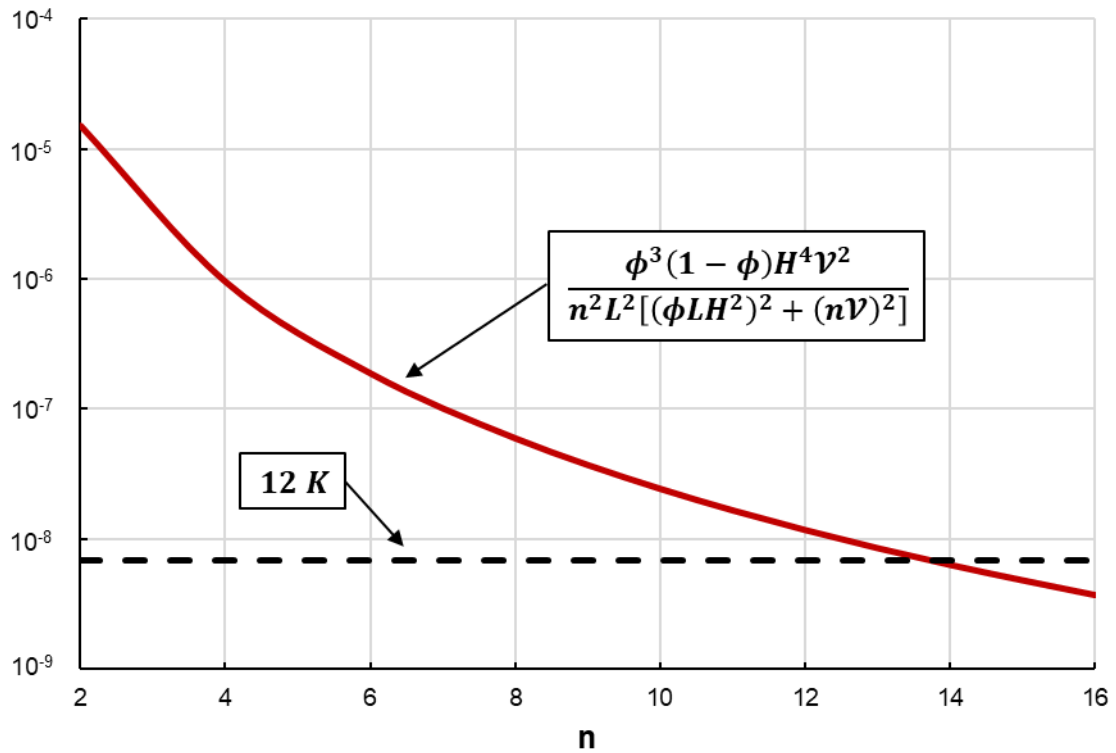


Figure 8 The two terms of Eq. 25 as a function of n .

For the sake of illustration, we show in Fig. 9 the heat release distribution for different values of the advancement ($n = 10$). The fluid enters from the left hand side of each figure (top left). This is where the chemical starts and propagates in times in the direction of the bottom right corner. Most of the heat release happens during the first 50 hours of the process, corresponding to an advancement of about 0.50. Obviously the values are dependent on the input data obtained from the experimental references; nevertheless they indicate a trend worth noticing.

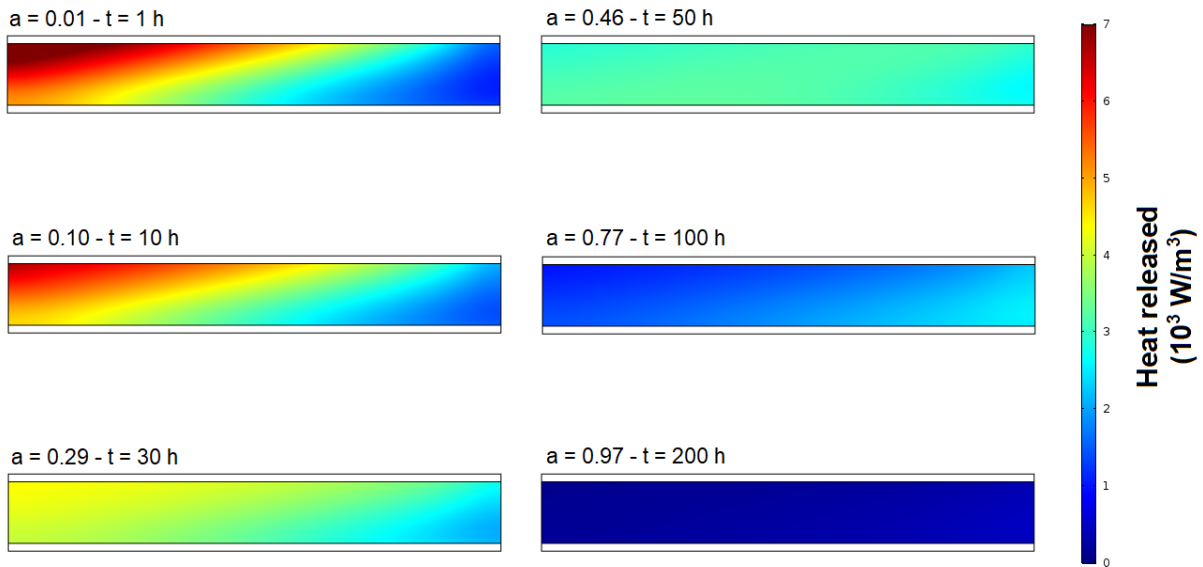


Figure 9 Heat released for different values of the reaction advancement ($n = 10$).

Next we compare the Constructal design of the module to numerical results obtained through a random search in which n , $\tilde{H} = H/L$ and $\tilde{W} = W/L$ were varied. The results are plotted in Fig. 10. This three-dimensional figure shows the overall performance β as a function of \tilde{H} and \tilde{W} for different numbers of salts beds. Figure 10 confirms that the path to better performance consists not only in increasing n , but also in configuring \tilde{H} and \tilde{W} . More details in the case $H = 12.5$ cm and $n = 10$ are provided in Fig. 11 where the numerical results from Fig. 10 were extracted and plotted as a function of H/W for different values of the advancement. The best configuration corresponds to $\tilde{H} = 1.25$, and $\tilde{W} = 0.8$, or said differently in Fig. 11, $\tilde{H}/\tilde{W} = 1.6$, departing from a cubical shape. Note that this result corresponds to what was earlier predicted through scale analysis invoking the Constructal law. Indeed in this case, Eq. 25 gives $\tilde{H}/\tilde{W} \sim 2.4$ in an order of magnitude sense.

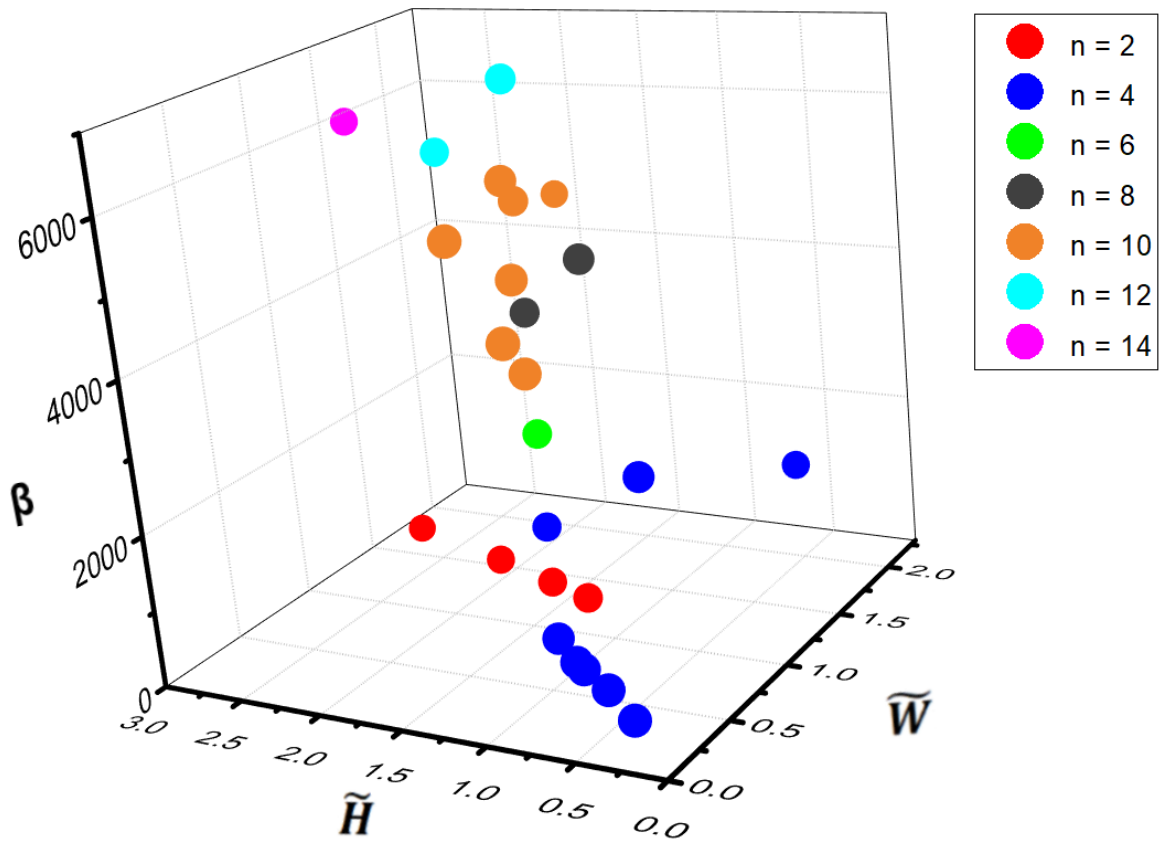


Figure 10 Ratio of heat released and pumping power, β , as a function of \tilde{H} , \tilde{W} and n , for multiple module configurations.

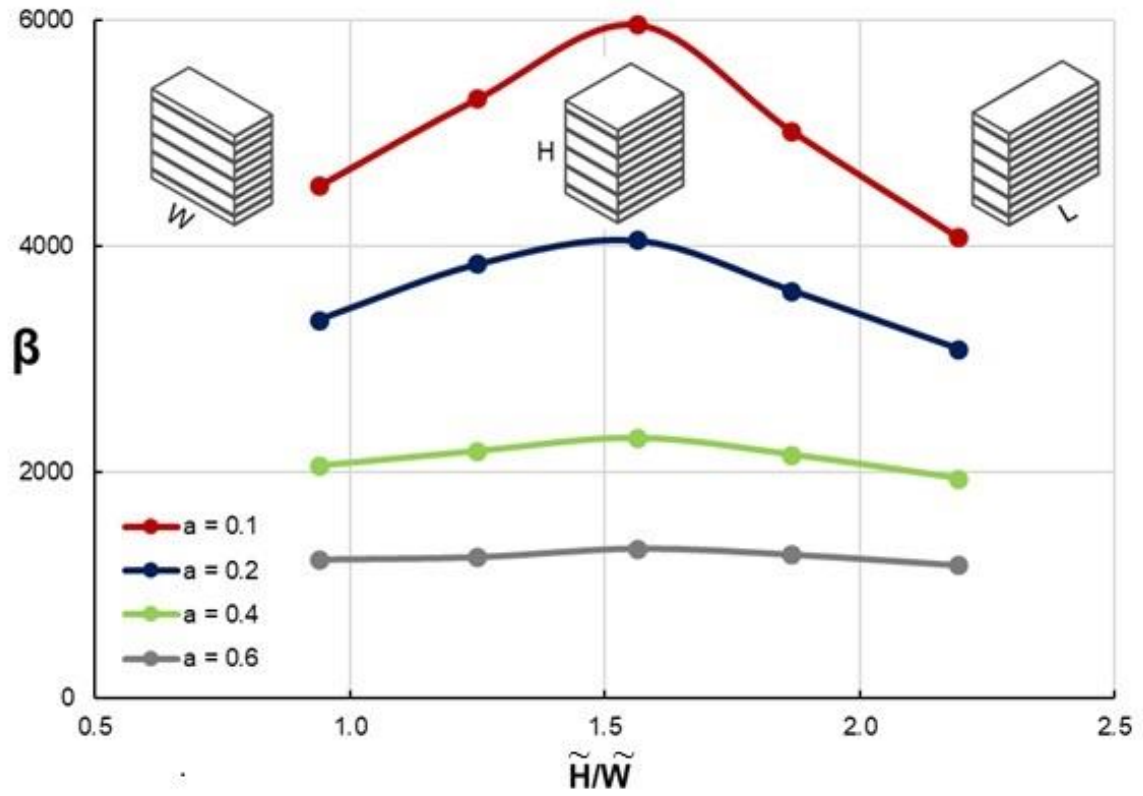


Figure 11 Ratio of heat released and pumping power, β , as a function of \tilde{H}/\tilde{W} , $n=10$ salt layers.

6. Concluding remarks

In this work we documented the Constructal design of a thermochemical energy storage module made of assemblies of parallel layers of reacting salt through which a heat transfer fluid conveyed by entrance and exit channels is blown. The main conclusion drawn by this study is that for a fixed value of the volume of the parallelepiped module and a fixed apparent porosity ϕ , increasing the number of parallel layers of salt allows to increase the overall performance of the system, namely the ratio between the heat released (or stored) and the power necessary to blow the fluid through the system. This result can be predicted from the Constructal law of design by searching for the equipartition of imperfections. We also learnt that Constructal design can be invoked in order to determine the shape of the module. The predicted aspect ratios were confirmed by a numerical search. The best configuration meets both compactness objectives and thermal/pumping power performances.

Acknowledgements

Alexandre Malley is funded by the French ANR research project DECARTH, ANR-16-CE22-0006-03.

REFERENCES

- [1] European Commission, COMMISSION STAFF WORKING DOCUMENT - Communication from the Commission to the European Parliament, the Council, the European Economic and Social Committee and the Committee of the Regions on an EU Strategy for Heating and Cooling, (2016). <http://ec.europa.eu/energy/en/topics/energy-efficiency/heating-and-cooling>.
- [2] K. Johannes, F. Kuznik, J.-L. Hubert, F. Durier, C. Obrecht, Design and characterisation of a high powered energy dense zeolite thermal energy storage system for buildings, *Appl. Energy*. 159 (2015) 80–86. doi:10.1016/j.apenergy.2015.08.109.
- [3] C. Finck, E. Henquet, C. van Soest, H. Oversloot, A.-J. de Jong, R. Cuypers, H. van't Spijker, Experimental Results of a 3 kWh Thermochemical Heat Storage Module for Space Heating Application, *Energy Procedia*. 48 (2014) 320–326. doi:10.1016/j.egypro.2014.02.037.
- [4] A. Fopah-Lele, C. Rohde, K. Neumann, T. Tietjen, T. Rönnebeck, K.E. N'Tsoukpoe, T. Osterland, O. Opel, W.K.L. Ruck, Lab-scale experiment of a closed thermochemical heat storage system including honeycomb heat exchanger, *Energy*. 114 (2016) 225–238. doi:10.1016/j.energy.2016.08.009.
- [5] A. Solé, I. Martorell, L.F. Cabeza, State of the art on gas–solid thermochemical energy storage systems and reactors for building applications, *Renew. Sustain. Energy Rev.* 47 (2015) 386–398. doi:10.1016/j.rser.2015.03.077.
- [6] B. Zettl, G. Englmaier, W. Somitsch, An Open Sorption Heat Storage Concept and Materials for Building Heat Supply, *Energy Procedia*. 73 (2015) 297–304. doi:10.1016/j.egypro.2015.07.692.
- [7] K.E. N'Tsoukpoe, T. Schmidt, H.U. Rammelberg, B.A. Watts, W.K.L. Ruck, A systematic multi-step screening of numerous salt hydrates for low temperature thermochemical energy storage, *Appl. Energy*. 124 (2014) 1–16. doi:10.1016/j.apenergy.2014.02.053.
- [8] B. Mette, H. Kerskes, H. Drück, Experimental and Numerical Investigations of Different Reactor Concepts for Thermochemical Energy Storage, *Energy Procedia*. 57 (2014) 2380–2389. doi:10.1016/j.egypro.2014.10.246.
- [9] C. Ferchaud, H. Zondag, R. de Boer, Material research on salt hydrates for seasonal heat storage application in a residential environment, ECN-M--13-022. (2013).
- [10] A. Bejan, Street network theory of organization in nature, *J. Adv. Transp.* 30 (1996) 85–107. doi:10.1002/atr.5670300207.
- [11] G. Lorenzini, C. Biserni, R.L. Correa, E.D. dos Santos, L.A. Isoldi, L.A.O. Rocha, Constructal design of T-shaped assemblies of fins cooling a cylindrical solid body, *Int. J. Therm. Sci.* 83 (2014) 96–103. doi:10.1016/j.ijthermalsci.2014.04.011.
- [12] L. Hermany, G. Lorenzini, R.J. Klein, F.F. Zinani, E.D. dos Santos, L.A. Isoldi, L.A.O. Rocha, Constructal design applied to elliptic tubes in convective heat transfer cross-flow of viscoplastic fluids, *Int. J. Heat Mass Transf.* 116 (2018) 1054–1063. doi:10.1016/j.ijheatmasstransfer.2017.09.108.
- [13] R.J. Klein, G. Lorenzini, F.S.F. Zinani, L.A.O. Rocha, Dimensionless pressure drop number for non-newtonian fluids applied to Constructal Design of heat exchangers, *Int. J. Heat Mass Transf.* 115 (2017) 910–914. doi:10.1016/j.ijheatmasstransfer.2017.07.122.
- [14] T.M. Gulotta, F. Guarino, M. Cellura, G. Lorenzini, Constructal law optimization of a boiler, *Int. J. Heat Technol.* 35 (Special Issue1) (2017) S261–S269. doi:10.18280/ijht.35Sp0136.
- [15] J. Ramalho, R. da Silva Brum, L.A.O. Rocha, L.A. Isoldi, E.D. dos Santos, M. Sulzbacher, Fitting new constructal models for the thermal potential of earth-air heat exchangers, *Acta Sci. Technol.* (2018) 1–8. doi:10.4025/actascitechnol.v40i1.30897.

- [16] D. Paludetto, S. Lorente, Modeling the heat exchanges between a datacenter and neighboring buildings through an underground loop, *Renew. Energy*. 93 (2016) 502–509. doi:10.1016/j.renene.2016.02.081.
- [17] S. Lorente, The Constructal law, from micro scale to urban scale design, *Annu. Rev. Heat Transf.* (2016) 335–368.
- [18] T. Watzek, S. Lorente, From pore network prediction based on the Constructal law to macroscopic properties of porous media, *J. Phys. Appl. Phys.* 48 (2015). doi:10.1088/0022-3727/48/48/485503.
- [19] S. Lorente, Constructal law applications to efficient design: electrokinetics systems and enclosures for heat transfer, *ASME J. Heat Transf.* 137 (2015). doi:10.1115/1.4029853.
- [20] A. Bejan, *The Physics of Life: The Evolution of Everything*, St. Martin's Press, New York City, 2016.
- [21] A. Bejan, Evolution in thermodynamics, *Appl. Phys. Rev.* (2017). doi:10.1063/1.4978611.
- [22] A. Bejan, S. Lorente, *Design with Constructal Theory*, Wiley, Hoboken, 2008.
- [23] K. Zhang, D. Zhao, Y. Zhai, X. Yin, R. Yang, G. Tan, Modelling study of the low-pump-power demand constructal T-shaped pipe network for a large scale radiative cooled-cold storage system, *Appl. Therm. Eng.* 127 (2017) 1564–1573. doi:10.1016/j.applthermaleng.2017.08.131.
- [24] S. Ziaei, S. Lorente, A. Bejan, Constructal design for convection melting of a phase change body, *Int. J. Heat Mass Transf.* 99 (2016) 762–769. doi:10.1016/j.ijheatmasstransfer.2016.04.022.
- [25] A. Bejan, S. Ziaei, S. Lorente, Distributed energy storage: Time-dependent tree flow design, *J. Appl. Phys.* 119 (2016) 184901. doi:10.1063/1.4948663.
- [26] M. Eslami, M.A. Bahrami, Sensible and latent thermal energy storage with constructal fins, *Int. J. Hydrog. Energy*. 42 (2017) 17681–17691. doi:10.1016/j.ijhydene.2017.04.097.
- [27] M. Sheikholeslami, S. Lohrasbi, D.D. Ganji, Response surface method optimization of innovative fin structure for expediting discharging process in latent heat thermal energy storage system containing nano-enhanced phase change material, *J. Taiwan Inst. Chem. Eng.* 67 (2016) 115–125. doi:10.1016/j.jtice.2016.08.019.
- [28] R. Kalbasi, M.R. Salimpour, Constructal design of horizontal fins to improve the performance of phase change material rectangular enclosures, *Appl. Therm. Eng.* 91 (2015) 234–244. doi:10.1016/j.applthermaleng.2015.08.024.
- [29] S. Lorente, Design of a Latent Thermal Energy Storage System From Constructal Approach, (2017) V008T10A063. doi:10.1115/IMECE2017-70594.
- [30] S. Lorente, A. Bejan, J.L. Niu, Constructal design of latent thermal energy storage with vertical spiral heaters, *Int. J. Heat Mass Transf.* 81 (2015) 283–288. doi:10.1016/j.ijheatmasstransfer.2014.09.077.
- [31] M. Abokersh, M. Osman, O. El-Baz, M. El-Morsi, O. Sharaf, Review of the phase change material (PCM) usage for solar domestic water heating systems (SDW HS), *Int. J. Energy Res.* (2018) 329–357. doi:1002/er.3765.
- [32] D.I. González, J. Amigo, S. Lorente, A. Bejan, F. Suarez, Constructal design of salt-gradient solar pond fields, *Int. J. Energy Res.* 40 (2016) 1428–1446. doi:10.1002/er.3.
- [33] A. Bejan, Fundamentals of exergy analysis, entropy generation minimization, and the generation of flow architecture, *Int. J. Energy Res.* 26 (2002) 0–43. doi:10.1002/er.804.
- [34] A. Bejan, *Convection heat transfer*, Second, John Wiley & Sons, Inc., 1995.
- [35] Michael J. Moran, Howard N. Shapiro, D.D. Boettner, M.B. Bailey, *Fundamentals of Engineering Thermodynamics*, 8th ed., 2014.

- [36] B. Michel, P. Neveu, N. Mazet, Comparison of closed and open thermochemical processes, for long-term thermal energy storage applications, *Energy*. 72 (2014) 702–716. doi:10.1016/j.energy.2014.05.097.
- [37] D.A. Nield, A. Bejan, *Convection in Porous Media*, second, Springer, 1998.
- [38] R.J. Millington, J.P. Quirk, *Permeability of porous media*, (1961).
- [39] H.L. Langhaar, Steady flow in the transition length of a straight tube, *J. Appl. Mech.* 64 (1942).
- [40] www.comsol.com, (n.d.).
- [41] B. Michel, N. Mazet, P. Neveu, Experimental investigation of an innovative thermochemical process operating with a hydrate salt and moist air for thermal storage of solar energy: Global performance, *Appl. Energy*. 129 (2014) 177–186. doi:10.1016/j.apenergy.2014.04.073.